Since January 2020 Elsevier has created a COVID-19 resource centre with free information in English and Mandarin on the novel coronavirus COVID-19. The COVID-19 resource centre is hosted on Elsevier Connect, the company's public news and information website.

Virology 549 (2020) 13–24

Contents lists available at ScienceDirect

Virology

journal homepage: www.elsevier.com/locate/virology

Mammalian orthoreovirus core protein μ2 reorganizes host microtubule-organizing center components

Catherine Eichwald*, Mathias Ackermann, Cornel Fraefel

Institute of Virology, University of Zurich, Winterthurerstrasse 266a, 8057 Zurich, Switzerland

ARTICLE INFO

Keywords:
Reoviridae
Microtubules
MTOC
μ2
μNS
Viral factories
γ-tubulin
Centrin

ABSTRACT

Filamentous mammalian orthoreovirus (MRV) viral factories (VFs) are membrane-less cytosolic inclusions in which virus transcription, replication of dsRNA genome segments, and packaging of virus progeny into newly synthesized virus cores take place. In infected cells, the MRV μ2 protein forms *punctae* in the enlarged region of the filamentous VFs that are co-localized with γ-tubulin and resistant to nocodazole treatment, and permitted microtubule (MT)-extension, features common to MT-organizing centers (MTOCs). Using a previously established reconstituted VF model, we addressed the functions of MT-components and MTOCs concerning their roles in the formation of filamentous VFs. Indeed, the MTOC markers γ-tubulin and centrin were redistributed within the VF-like structures (VFLS) in a μ2-dependent manner. Moreover, the MT-nucleation centers significantly increased in numbers, and γ-tubulin was pulled-down in a binding assay when co-expressed with histidine-tagged-μ2 and μNS. Thus, μ2, by interaction with γ-tubulin, can modulate MTOCs localization and function according to viral needs.

1. Introduction

During early times post-infection, as part of the primary transcription payload, mammalian orthoreovirus (MRV) forms small, membrane-less, punctuated cytosolic inclusions named viral factories (VFs). As the virus protein levels increase with the secondary transcription, the VFs enlarge and localize to the perinuclear area. Several biochemical processes occur within the VFs, such as the synthesis of ss (+) RNAs both for translation and as templates for replicating dsRNA genome segments, which are subsequently packaged in newly formed viral cores. Several MRV proteins compose VFs including μ2, μNS, μNSC, σNS, λ2, μ3 as well as an undetermined number of host proteins such as microtubules (MTs) (Parker et al., 2002), TRiC chaperonin (Knowlton et al., 2018), dynein (Eichwald et al., 2018), clathrin (Ivanovic et al., 2011) and HSC70 (Kaufer et al., 2012). Depending on the virus strain, the VFs are filamentous (e.g., T1L strains) or globular (e.g., $T3D^N$); the diversification mainly depends on the ability of minor core protein μ2 to associate with MTs (Broering et al., 2002; Eichwald et al., 2017; Miller et al., 2004; Parker et al., 2002). Specifically, a μ2 point mutation in Pro 208 to Ser predisposes to the formation of globular VFs (Parker et al., 2002). Additionally, μ2 needs to self-oligomerize for MT-association through aa region 283–325 (Eichwald et al., 2017). Interestingly, μNS, when expressed in the absence of other viral proteins forms cytosolic inclusions (Arnold et al., 2008; Broering et al., 2004) termed VF-like structures (VFLS) that are morphologically identical to globular VFs. When μ2 (T1L; aa region 290–435) interacts with μNS, filamentous VFLSs are formed (Broering et al., 2002; Eichwald et al., 2017). VFs are highly dynamic structures that coalesce with each other and move to the perinuclear area. These processes require at least dynein as a molecular motor (Eichwald et al., 2018). Since the study of filamentous VF dynamics turns to be cumbersome, a reconstituted model based on the transfection of different ratios of μ2-and μNS-encoding plasmids (μ2/μNS) allowed providing simplified elements for quantification of diverse motion events. This model mimics different stages of VF dynamics at increasing time post-infection (Eichwald et al., 2018).

MTs are polarized polymers composed of α- and β-tubulin heterodimers with a length ranging from 1 to 100 μm and dependent on GTP for their assembly. The MTs provide the track for motors allowing the movement of organelles, vesicles, and other structures, which contributes to the efficient functioning of the cells and the organism (Goodson and Jonasson, 2018). Thus, MTs play a role in the cell organization as they are involved in organelle localization and in establishing cell polarity. MTs undergo a series of post-translational modifications (PTMs), including phosphorylation, acetylation, sumoylation, detyrosination, and polyglutamylation (Janke and Bulinski, 2011).

* Corresponding author.
E-mail addresses: ceichwald@vetvir.uzh.ch (C. Eichwald), mathias.ackermann@uzh.ch (M. Ackermann), cornel.fraefel@vetvir.uzh.ch (C. Fraefel).

https://doi.org/10.1016/j.virol.2020.07.008
Received 24 April 2020; Received in revised form 2 July 2020; Accepted 8 July 2020
Available online 04 August 2020

While most tubulin PTMs occur on the outer surface of MTs, acetylation has been identified in Lys 40 of α-tubulin, which is exposed at the MT-luminal inner surface (L'Hernault and Rosenbaum, 1985; LeDizet and Piperno, 1987; Piperno et al., 1987; Soppina et al., 2012). Drugs such as taxol (Alushin et al., 2014) and low temperature stabilize MTs, whereas other drugs such as nocodazole, colchicine, vinblastine, and vincristine depolymerize the MTs (Goodson and Jonasson, 2018). MT-organizing centers (MTOCs) are the general term for all localized foci of the MT-nucleating machinery, including centrosomes and spindle pole bodies (Vertii et al., 2016). MTOCs contain γ-tubulin and the γ-tubulin ring complex (γ-TURC) as well as centrioles and a complex array of other proteins, such as motors and +TIP (MT plus-end tracking protein). The γ-tubulin, present in all eukaryotic organisms, is a key element of the cytoskeleton that nucleates the growth of new MT structures (Zheng et al., 1995). It arranges in a helical manner at the edge of the γ-TURC cap to form strong longitudinal contacts with the incoming α-tubulin of αβ-tubulin heterodimers, thereby providing a template for the formation of 13 protofilament MTs (Aldaz et al., 2005; Kollman et al., 2010). Other proteins also have a role in the MT-nucleation. For example, centrin is a main component of centrioles that links MT-doublets and plays a role in both spatial and temporal control over centrioles (Salisbury, 2007). Interestingly, MT-severing enzymes cut pre-existing MTs, creating new MT ends that can serve as γ-TURC-independent platforms for templated MT-nucleation, which appears a relevant process in mammalian neurons, plants, and nematodes (Baas and Ahmad, 1992; Lindeboom et al., 2013; Srayko et al., 2006).

Here, specific μ2 *punctae* observed in filamentous VFs are investigated concerning their ability to co-localize with other reovirus proteins and host elements. Our study shows that μ2 *punctae* in VFs co-localize with γ-tubulin, are resistant to nocodazole, and permit MT emergence, common features for MTOCs. Moreover, using the VFLS model, we found that specific μ2/μNS ratios that support filamentous morphology relocalize γ-tubulin and centrin to foci within the VFLS. Such association is obliterated upon MT overexpression.

2. Results

2.1. Filamentous viral factories have MTOC-like structures

Immunofluorescence microscopy of reovirus T1L infected cells at 12 hpi, revealed μ2 *punctae* inside the filamentous VFs (Fig. 1A). The *punctae* co-localized neither with other viral proteins (μNS, σNS, λ2, σ3, μ1) **(**Fig. 1B–E **and** Fig 2A**)** nor with intermediate filaments or dynein intermediate chain (DIC) (Fig. 2D and E). Co-staining for μ2 and α-tubulin, however, showed bundles of MTs extending from the *punctae*, suggesting that the *punctae* may have a role as MTOCs (Fig. 2C). Indeed, co-staining for μ2 and γ-tubulin, a conventional marker for centrosomes and other MTOCs (Roostalu and Surrey, 2017), showed μ2 and γ-tubulin co-localizing in the *punctae* as denoted by immunofluorescence photomicrograph and profile intensities of the linear region of interest (LROI) (Fig. 2B). Importantly, nocodazole treatment, which is a well-known MT-depolymerizing agent, failed to disrupt the *punctae*, which remained positive for both μ2 and γ-tubulin **(**Fig. 3A and B**).** Our results show that γ-tubulin localization is intensified in μ2 *punctae* upon nocodazole treatment (Fig. 3D), consistent with the fact that MTOCs are nocodazole resistant (Rogalski and Singer, 1984). Reovirus protein μNS is mainly dispersed from *punctae* when cells are treated with nocodazole (Fig. 3A), suggesting a mild or no role in μ2 *punctae* formation. As expected, MT bundles depolymerized upon nocodazole treatment **(**Fig. 3C**).**

2.2. MTOC-like structures in filamentous viral factories are nocodazole resistant

T1L-infected cells were treated with 10 μM nocodazole from 1 to 12 hpi, a treatment that does not disturb the virus entry process (Eichwald et al., 2018; Mainou and Dermody, 2011; Mainou et al., 2013). Nocodazole was then removed from the medium, allowing MTs to re-polymerize for 0, 5, 15, 30, or 60 min before methanol-fixation (Fig. 4A). Immediately after nocodazole removal (i.e., at 0 min), μ2-*punctae* were observed in the VFs while filamentous μ2 and MTs were not. However, within only 15 min after nocodazole removal, polymerizing MTs with associated μ2 were observed extending from the *punctae* (Fig. 4B, C, and D). These findings strongly suggest that the *punctae* in the viral factories are functionally MTOC-like and may nucleate MTs and direct MT formation in cells.

2.3. γ-tubulin and centrin form punctae within μ2(T1L)/μNS-VFLSs

We recently described that the reconstitution of VFLS upon transfection of expression plasmids encoding μ2 (T1L) and μNS at different ratios (μ2/μNS) may serve as a model for studying temporal dynamics of VFs (Eichwald et al., 2018). MTOCs are visualized as two *punctae* at a juxtanuclear position during interphase (Lüders and Stearns, 2007; Sanchez and Feldman, 2017). Under this consideration, we investigated the localization of two specific markers for MTOCs, specifically γ-tubulin **(**Fig. 5**)** and centrin **(**Fig. 6**)**. As expected, at non-transfected (NT) conditions, both γ-tubulin and centrin localized to well-featured MTOCs corresponding to two polarized *punctae* at the perinuclear area **(**Figs. 5 and 6**, lower row)**. Similarly, γ-tubulin and centrin in cells containing VFLS formed at ratios 2:0, 2:4, and 0:4 of μ2/μNS **(**Figs. 5 and 6**, first, fourth, and fifth rows)** mainly localized in MTOCs. In contrast, γ-tubulin and centrin localized to defined *punctae* in VFLS reconstituted with μ2/μNS transfection ratios of 2:1 and 2:2 **(**Figs. 5 and 6**, second and third rows)**. To evaluate if γ-tubulin and centrin *punctae* increment in number and redistribute to VFLSs generated with different μ2/μNS ratios, we first quantified cells with more than two γ-tubulin *punctae*. As denoted in Fig. 7A, a significantly higher percentage of cells containing > 2 MTOCs is observed at 2:1 and 2:2 transfection ratios of μ2 (T1L)/μNS when compared to the other ratios. Similar results were obtained when quantifying the localization of centrin labeled *punctae* (Fig. 7B). To analyze the redistribution of MTOC-like *punctae*, we performed three-dimensional (3D) reconstructions of Z-stack images acquired by high definition confocal microscopy. The 3D-reconstruction VFLSs formed with μ2 (T1L)/μNS at transfection ratio of 2:1 (Fig. 7C, C′ and C″) showed that centrin *punctae* co-localize with the μ2 signal in VFLS, suggesting the redistribution of the MTOC-like *punctae* among VFLSs. Interestingly, μ2 association to MTs role seems pre-requisite since μ2 ($T3D^N$)/μNS VFLS is defective for γ-tubulin recruitment when compared to μ2 (T1L)/μNS VFLS at any of the studied ratios (Fig. S1).

Consistent with our results, γ-tubulin-HA was pulled down from an extract of cells previously transfected with expression plasmids encoding HA-tagged γ-tubulin and μ2-H_{6X} (histidine tag)/μNS at a transfection ratio of 2:1 **(**Fig. 7D**, lane 6)**. Meanwhile, weak or no association of γ-tubulin-HA was observed at transfection ratios 2:0, 2:2, and 2:4 **(**Fig. 7D**, lanes 3, 9, and 12)**.

2.4. Centrin punctae in VFLS delocalize upon MT-overexpression

Next, we investigated whether MT-overexpression reduces MTOC-like localization in VFLSs. For this purpose, we over-expressed β-tubulin-mCherry (Matov et al., 2010) or mCherry in cells with VFLSs reconstituted with a μ2/μNS transfection ratio of 2:1. We used this specific μ2 (T1L)/μNS VFLS ratio because the above experiments (Figs. 5–7) indicated more MTOC-like structures among VFLS**.** As observed in Fig. 8A, when VFLSs are reconstituted with a μ2 (T1L)/μNS transfection ratio of 2:1, the over-expression of MTs (β-tubulin-mCherry) resulted in a significant decrease in the percentage of cells containing > 2 MTOCs when compared with the control (mCherry). Interestingly, the expression of β-tubulin-mCherry or mCherry did not alter the number of MTOCs in cells with no VFLSs (NT) (data not shown). Also, VFLSs composed of μNS only were not affected by the

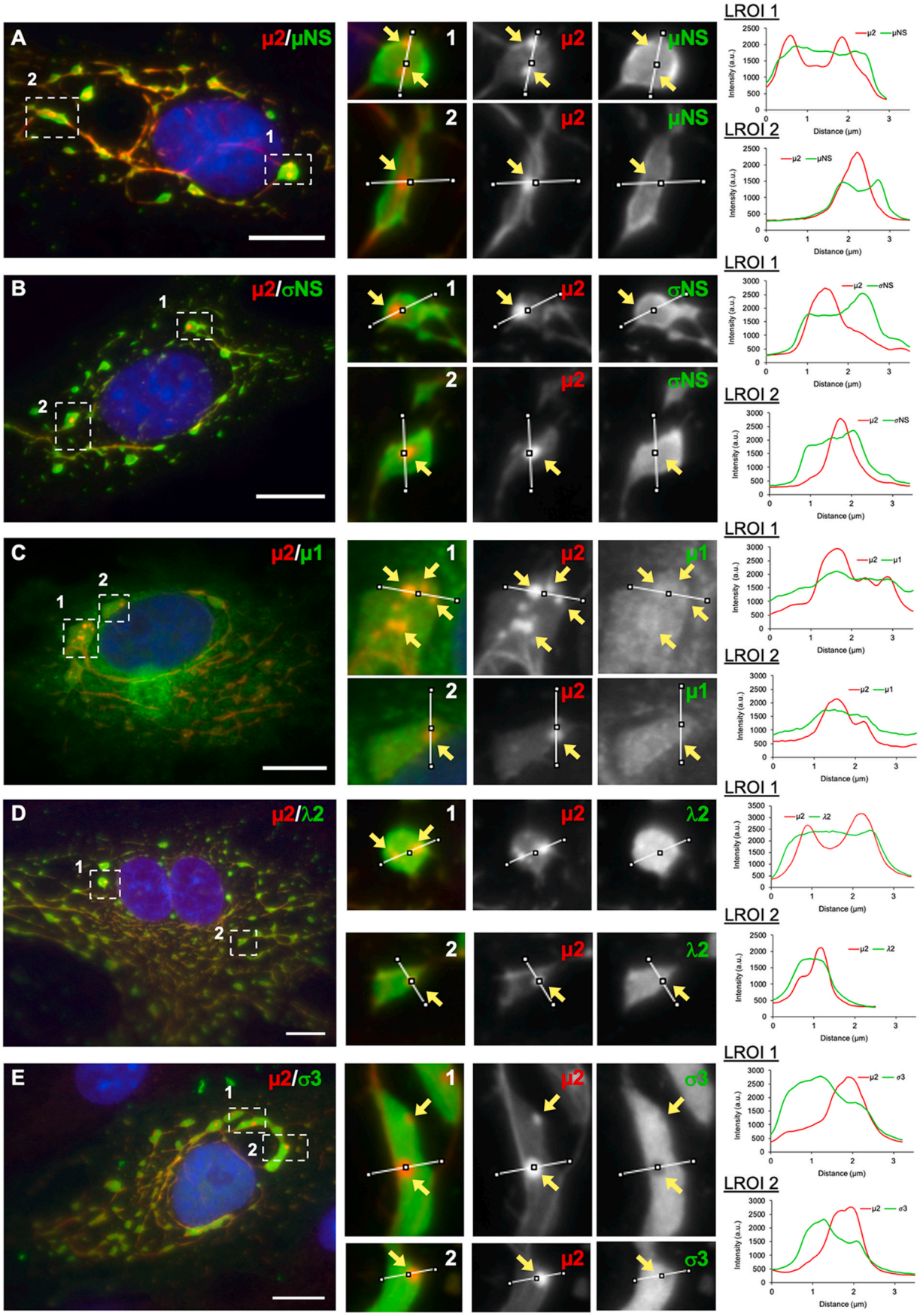

Fig. 1. μ2 forms *punctae* in T1L induced VF inclusions. CV-1 cells were infected with MRV T1L at an MOI of 10 pfu/cell. At 12 hpi, cells were fixed and immunostained for the detection of μ2 (anti-μ2-Texas red, red), μNS (A), σNS (B), μ1 (C), λ2 (D), and σ3(E) (green). Nuclei were stained with DAPI (blue). The dashed open boxes correspond to the magnified images in the right panel. The yellow arrowheads indicate the position of μ2 *punctae* in VFs. Scale bar is 10 μm. Intensity profile plot of μ2 *punctae* (red line) and indicated proteins (green line) of the linear region of interest (LROI) of images from the corresponding open box of each image panel.

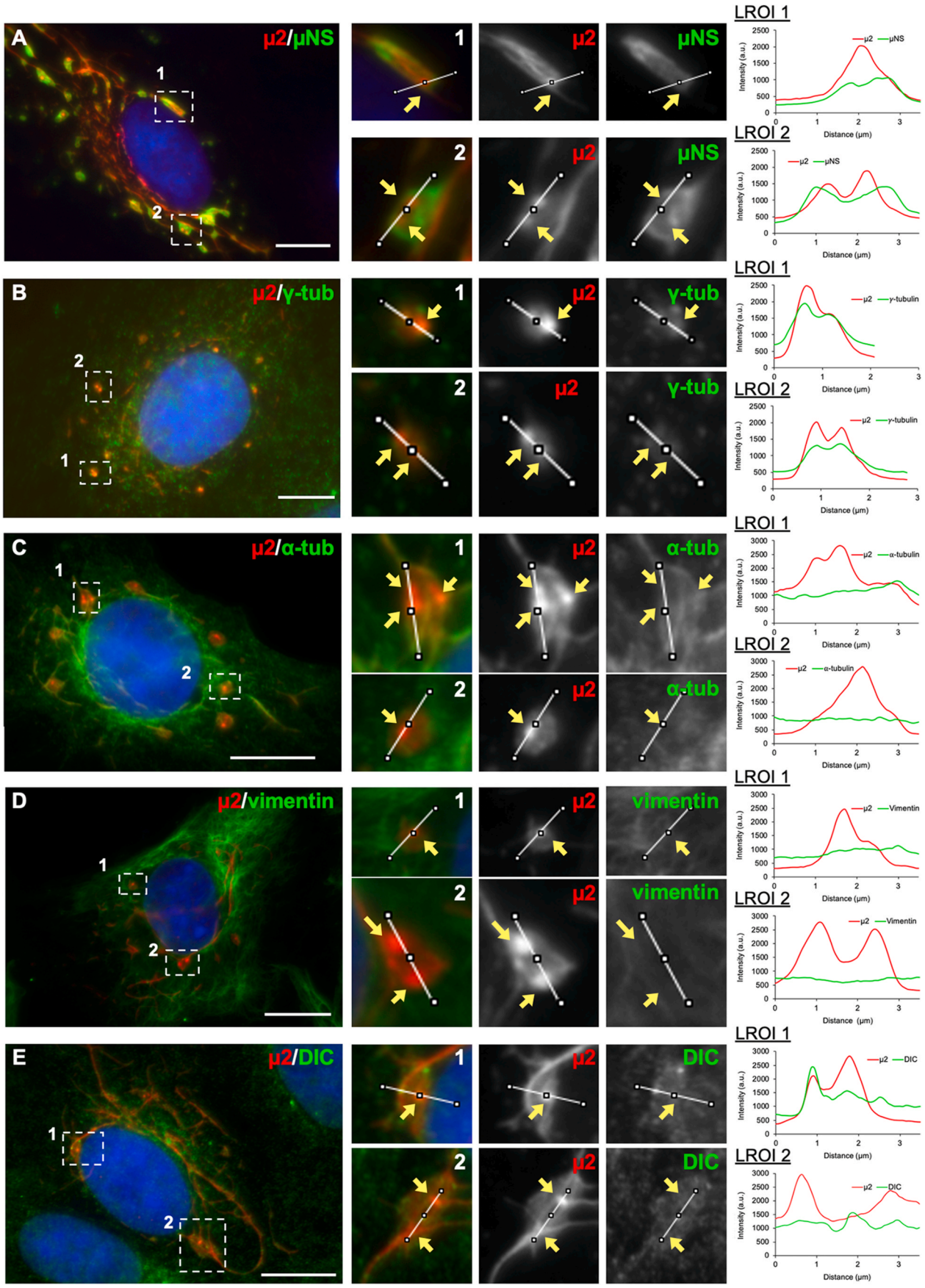

(caption on next page)

Fig. 2. γ-tubulin localizes within μ2 puncta. Immunofluorescence of MRV T1L-infected CV-1 cells [MOI, 10 pfu/cell]. At 12 hpi, cells were fixed and immunostained for the detection of μ2 (anti-μ2-Texas Red, red), μNS (A) (anti-μNS-Alexa 488, green), γ-tubulin (B) (anti-γ-tubulin, green), MTs (C) (anti-α-tubulin, green), intermediate filaments (D) (anti-vimentin, green) and dynein (E) (anti-dynein intermediate chain (DIC), green). Nuclei were stained with DAPI (blue). The dashed open boxes correspond to the localization of the magnified images in the right panel. The yellow arrowheads indicate the position of μ2 *punctae* in VFs. Scale bar is 10 μm. Intensity profile plot of μ2 *punctae* (red line) and indicated proteins (green line) of the linear region of interest (LROI) of images from the corresponding open box of each image panel.

increasing number of MTs. Moreover, as denoted in Fig. 8B, an increase in MTs (β-tubulin-mCherry) seems to favor the perinuclear condensation of VFLS compared to the mCherry control. Consistent with a previous report (Eichwald et al., 2018), the perinuclear condensation of VFLS composed only of μNS was not impaired by an increase in the number of MTs. This outcome confirms that μNS plays no role in VF perinuclear condensation.

3. Discussion

The formation of μ2 *punctae* in filamentous VFs is not a novel observation; these structures have been described previously as putative replication centers in VFs (Parker et al., 2002). However, μ2 *punctae* linked to the MRV replication center were indirectly supported by the μ2 functions as structural minor core protein (Coombs, 1996; Wiener et al., 1989), NTPase (Noble and Nibert, 1997), and RTPase (Kim et al., 2004). Here, we show evidence that μ2 *punctae* instead are MTOC-like structures recruiting γ−tubulin and centrin to the VFs. The μ2 *punctae* did neither co-localize properly with any of the other MRV proteins that are VF components nor with α-tubulin or dynein intermediate chain, which are known host components of VFs (Eichwald et al., 2018; Parker et al., 2002). The resistance of the μ2 *punctae* to nocodazole treatment, an MT-depolymerizing drug, is a well-established feature of MTOC-like structures (Zheng et al., 1995). Another MTOC behavior is the ability to nucleate MTs (Kollman et al., 2010). We show that cells reconstituted from nocodazole treatment supported MT-reemergence from μ2 *punctae*. Indeed, as μ2 directly associated with MTs (Kim et al., 2004), it also reemerged with MTs from the VF MT-nucleation center. Interestingly, our data is consistent with the presence of μ2 *punctae* in globular VFs formed, e.g., in strain $T3D^N$, since μ2 of this strain cannot associate with MTs (Broering et al., 2002, 2004; Eichwald et al., 2017, 2018; Miller et al., 2003; Parker et al., 2002) but could still interact with MTOC components as γ-tubulin. As described previously (Eichwald et al., 2018), globular VF dynamics are also dependent on intact MT-network, including MT-nucleation and orientation. Since μ2 ($T3D^N$) VFLSs show defective γ-tubulin recruitment, it suggests *i)* the requirement, aside from μNS, of other host or viral components and *ii)* MT-association region of μ2 is not sufficient for γ-tubulin recruitment. This topic is currently under investigation in our laboratory. These outcomes are also consistent with the VFLS simplified model using different μ2 (T1L)/μNS expression plasmid ratios, which allowed us to determine that a reduced amount of μNS is required for the recruitment γ-tubulin and centrin. This outcome is not surprising since it has previously been demonstrated that μNS stabilizes the μ2-MT association (Eichwald et al., 2018). However, μNS is unable to recruit the MTOC components into VFLS, suggesting a predominant role of μ2. These results have been demonstrated by employing high definition confocal immunofluorescence microscopy, quantification of MTOCs, and pull-down of γ−tubulin-HA, and consistently revealed that a μ2/μNS expression plasmid ratio of 2:1 supports both MT nucleation in VFLSs and association with γ-tubulin. An overexpression of MTs, as obtained upon transfection of β-tubulin-mCherry, impaired the MT-nucleation in VFLS even at a μ2/μNS ratio of 2:1, indicating a competence between μ2 and host components for the association to MTOC components. Interestingly, VFLSs at ratio 2:1 condensate at the perinuclear region faster when MTs are overexpressed than in control conditions (mCherry). This effect is explained by favoring the direct association of μ2-MT (Eichwald et al., 2017; Parker et al., 2002) over the μ2/μNS association (Eichwald et al., 2018; Miller et al., 2010). Thus, it has been described that VFLS composed of μ2 only condenses better at the perinuclear area than VFLS generated μ2/μNS transfection ratio 2:1 (Eichwald et al., 2018). Here, we also show that the μ2-VFLS (ratio 2:0) preserves the juxtanuclear MTOC position, indicating that μ2 may associate with MT and move towards MT with the help of an unknown kinesin. As expected and consistent with our previous work (Eichwald et al., 2018), μNS VFLS (ratio 0:4) did not alter its localization in the presence of an excess of MT confirming no MT-association.

Importantly, filamentous MRV is not the first case of MTOC subversion. Several viruses have usurped MTOCs properties to favor their replication. For example, human cytomegalovirus (HCMV) forms a Golgi based MT-nucleation center to facilitate virus assembly (Procter et al., 2018). Herpes simplex virus-1 favors non-centrosomal MT nucleation to promote efficient virus spread (Pasdeloup et al., 2013). Human immunodeficiency virus (HIV-1) accumulates MTOCs at the pre-integration step, elongating the centrosomes and recruiting γ-tubulin by a role attributed to Vpr (Hossain et al., 2018). Other viruses, such as poxviruses or African swine fever virus (ASFV), create VFs at MTOCs (Wileman et al., 2016). β-coronaviruses, including SARS-CoV, adapt their replication vesicles surrounding MTOCs (Angelini et al., 2013). However, this is the first report showing that cytosolic membrane-less factories can recruit MT-nucleation centers. These MTOC-like structures are mainly found in the enlarged globular part of the filamentous VFs. Thus, several roles could be attributed to MTOC-like structures: i) support of genome packing by MT-network (Shah et al., 2017) and ii) transition of VFs towards the perinuclear region to favor interchanges with the nucleus. In this sense, μ2 has been described to localize in the nucleus (Zurney et al., 2009) and to trigger innate immunity (Irvin et al., 2012; Stebbing et al., 2014). These exciting alternatives require further investigation.

In summary, μ2 *punctae* behave like MTOCs by nucleating MTs into VFs. Also, MTOCs standard markers, γ-tubulin, and centrin get recruited into both VFs and VFLSs. The VF matrix μNS did not have a direct role in μ2 *punctae* formation; however, it supported MTOC components, at least in a VFLS model.

4. Materials and methods

4.1. Cells and viruses

CV-1 cells (African green monkey fibroblasts) were obtained from Max L. Nibert's stock and cultured in Dulbecco's modified Eagle's medium (Invitrogen) supplemented with 10% fetal bovine serum [ANIMEB, Bioconcept, Switzerland] and penicillin/streptomycin. MRV strain T1L and $T3D^N$ was obtained from the Bernard N. Fields collection, kindly provided by Max L. Nibert (Harvard Medical School, Boston, MA). Viral titers were determined by plaque assay using L-cell monolayer (Tyler et al., 1985). T_7 RNA polymerase recombinant vaccinia virus (strain vvT7.3) was amplified, and viral titer determined as described previously (Fuerst et al., 1986).

4.2. Antibodies and reagents

Rabbit polyclonal antisera specific for μ2 and μNS were used as described previously (Parker et al., 2002; Rhim et al., 1962). Rabbit polyclonal anti-μNS conjugated to Alexa 488 and rabbit polyclonal anti-μ2 conjugated to Texas-red were described previously (Broering et al.,

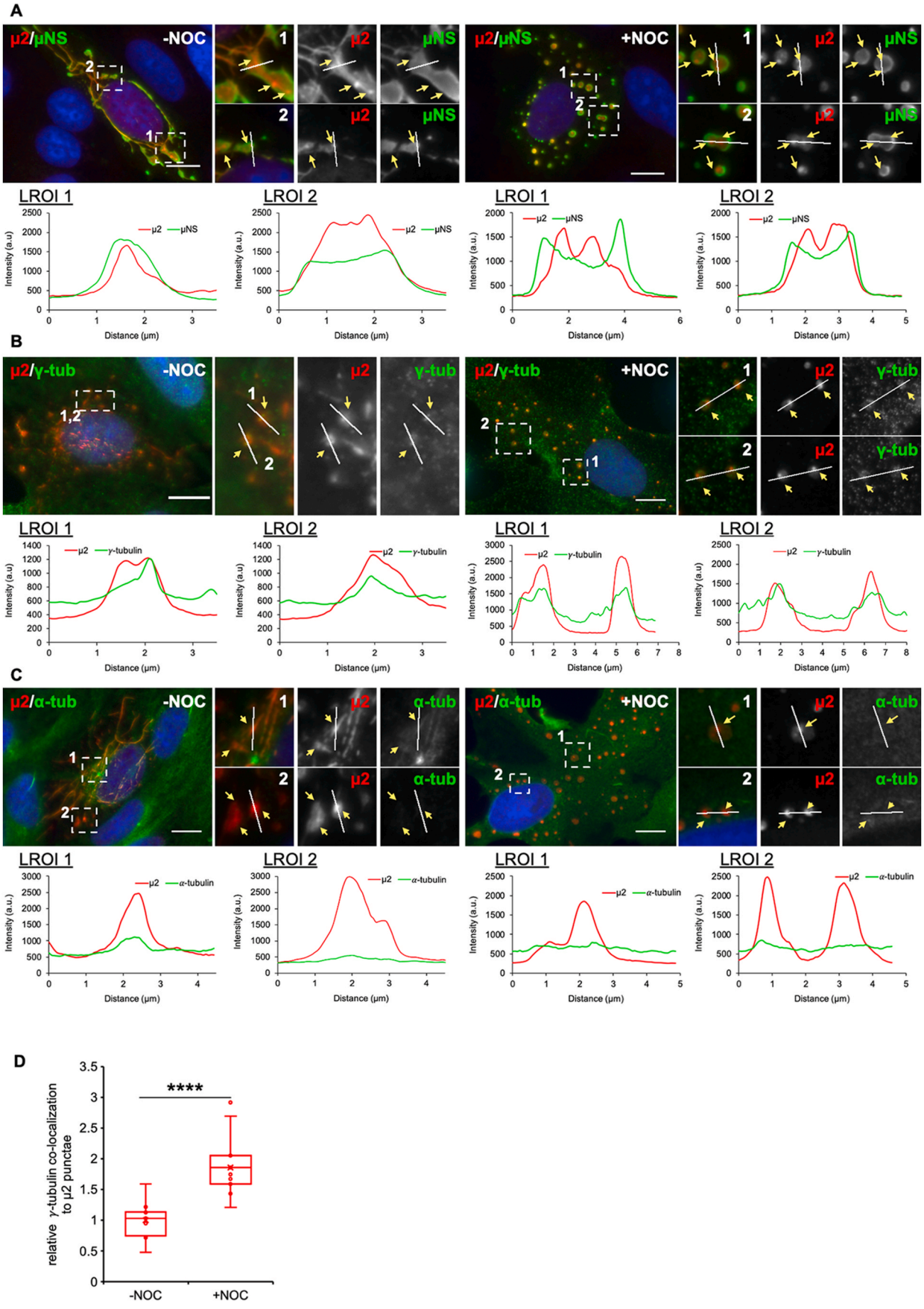

(caption on next page)

Fig. 3. μ2 *punctae* are resistant to nocodazole treatment and co-localize with γ-tubulin. Immunofluorescence of MRV T1L (MOI, 10 pfu/cell)-infected CV-1 cells, either untreated (-NOC, left panel) or treated with 10 μM nocodazole (+NOC, right panel) for 2 h before fixation. At 18 hpi, cells were fixed and immunostained for the detection of μ2 (anti-μ2-Texas red, red), μNS (A) (anti-μNS-Alexa 488, green), γ-tubulin (B) (anti-γ-tubulin, green) and MTs (C) (anti-α-tubulin, green). Nuclei were stained with DAPI (blue). The dashed open white boxes correspond to magnified images in each panel on the middle column. The yellow arrows indicate the position of the μ2 *punctae* in VFs. Scale bar is 10 μm. Intensity profile plot of μ2 *punctae* (red line) and indicated proteins (green line) of the linear region of interest (LROI) of images from the corresponding open box of each image panel. (D) Box plot of relative co-localization to μ2 *punctae* with γ-tubulin untreated (-NOC) or treated with nocodazole (+NOC). Data is presented as median ± quartile; *t*-test, (****) $p < 0.0001$, $n > 15$ μ2 *punctae*.

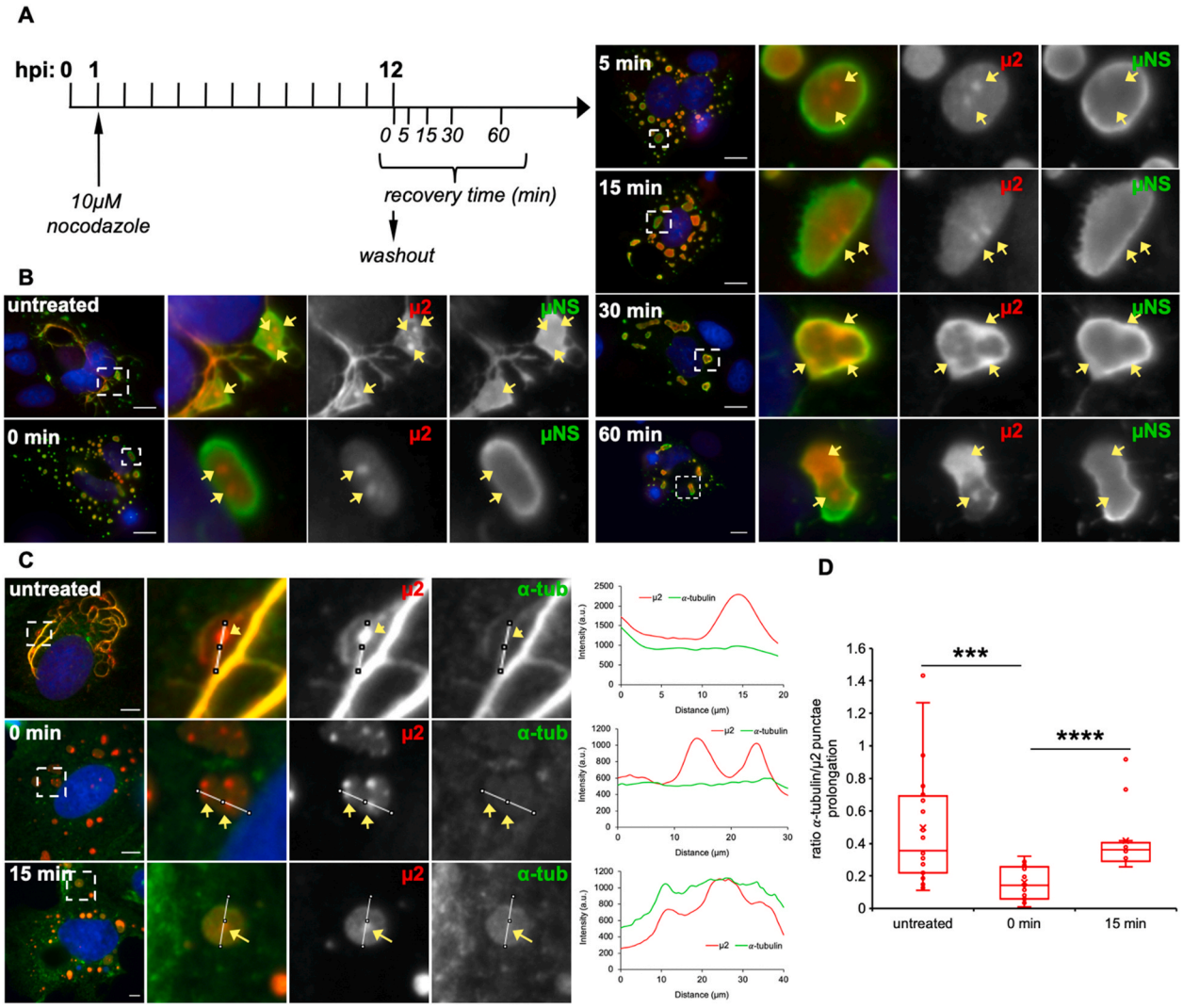

Fig. 4. μ2 *punctae* act as MTOC-like structures. (A) Experimental-design for MT recovery in MRV-infected cells after treatment with nocodazole. (B and C) Immunofluorescence detection of μ2 *punctae* in VF at the indicated times post-recovery after nocodazole treatment. MRV-infected cells were fixed and immunostained for the detection of μ2 (anti-μ2-Texas Red, red), μNS (B) (anti-μNS-Alexa 488, green) and MTs (C) (anti-α-tubulin, green). Nuclei were stained with DAPI (blue). The dashed open white boxes correspond to magnified images in the right panel. The yellow arrows point to the localization of the yellow arrows. Scale bar is 10 μm. Intensity profile plot of μ2 (red line) and α-tubulin (green line) of the linear region of interest of images from nocodazole untreated (top panel), 0 min– (middle panel) and 5 min-(bottom panel) recovery of nocodazole treatment. (D) Box plot of α-tubulin and μ2 *punctae* prolongation at indicated conditions. Data is presented as median ± quartile; *t*-test, (***) $p < 0.001$, (****) $p < 0.0001$, $n > 15$ μ2 *punctae*.

2004). Mouse monoclonal antibody (mAb) anti-σNS (3E1) (Becker et al., 2001), mouse mAb anti-μ1 (clone 10H2) (Chandran and Nibert, 1998), mouse mAb anti-λ2 (clone 7F4) (Virgin et al., 1991), and mouse mAb anti-σ3 (clone 5C3) (Broering et al., 2002) were published previously. Mouse mAb anti-γ-tubulin (C-11) and mouse anti-vimentin were purchased from Santa Cruz Biotechnology. Mouse mAb anti-centrin (clone 20H5) was purchased from Millipore. Mouse mAb anti-α-tubulin (clone B-5-1-2), mouse monoclonal anti-dynein intermediate chain (clone 70.1), mouse mAb anti-γ-tubulin (clone GTU-88) and mouse anti-HA (clone HA-7) were purchased from Sigma-Aldrich. Goat anti-mouse immunoglobulin G (IgG) conjugated to Alexa 488, goat anti-rabbit IgG conjugated to Alexa 594, and goat anti-mouse IgG conjugated to Alexa 647, were obtained from Molecular Probes, Invitrogen. Nocodazole was purchased at Sigma-Aldrich.

4.3. DNA plasmids

pCI-μ2 (T1L), pCI-μ2 ($T3D^N$), and pCI-μNS(T1L) were previously described (Broering et al., 2002; Parker et al., 2002). pCI-μ2 (T1L)-H_{6X} was obtained by PCR amplification of pCI-μ2 (T1L)-HA (Eichwald et al., 2017) using specific primers to insert flanking *Xho*I/histidine tag-*Not*I sites, followed by ligation between the *Xho*I and *Not*I sites of pCI-Neo

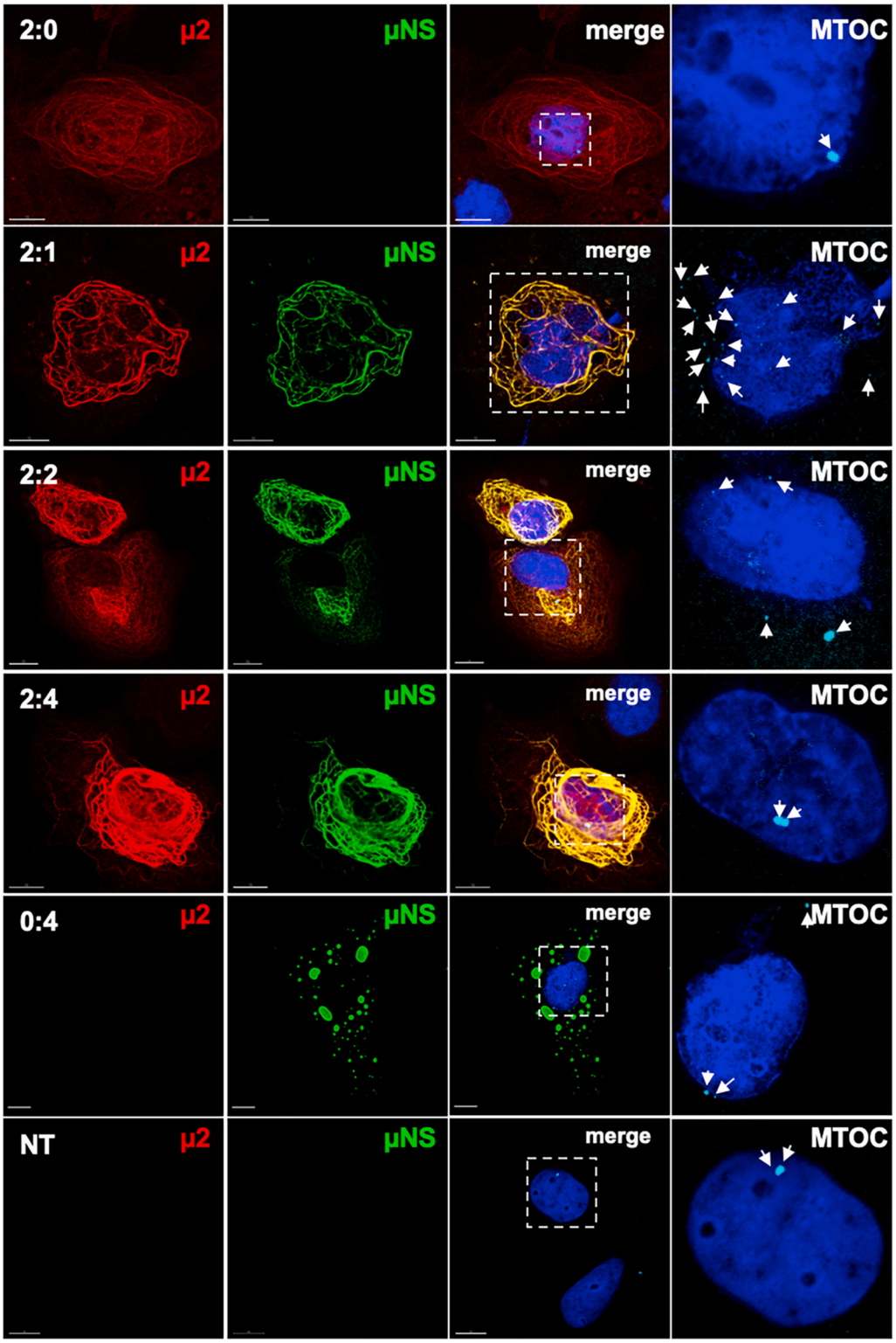

Fig. 5. γ-tubulin redistributes into VFLSs. Confocal maximum intensity projection of VFLSs immunofluorescence composed of the indicated transfection ratios μ2 and μNS expression plasmids. At 24 hpt, CV-1 cells were fixed with methanol and immunostained with specific antibodies for the detection of μ2 (red), μNS (green), and γ-tubulin (cyan). Nuclei were stained with DAPI (blue). The third column shows a merged image. The dashed white open boxes correspond to magnified images in the fourth column. White arrowheads point to γ-tubulin localization. NT, non-transfected cells. Scale bar is 10 μm.

(Promega). pcDNA-γ-tubulin-HA was obtained by PCR amplification of pcDNA-human γ-tubulin-EGFP using specific primers to insert flanking *Xho*I/HA-tag-*Not*I sites, followed by ligation in those sites in pCI-Neo (Promega). pcDNA-human γ-tubulin-EGFP was kindly provided by Karl Munger (Harvard Medical School, Boston, MA, USA) (Nguyen et al., 2007). pCI-β-tubulin-mCherry was obtained by PCR amplification of β-tubulin from pTUBB-EGFP (Akoumianaki et al., 2009), kindly provided by Urs Greber (University of Zurich, Zurich, Switzerland), using specific primers to insert flanking *EcoR*I/*Sal*I restriction sites, followed by ligation in those sites in pCI-mCherry-stop. pCI-mCherry-stop was

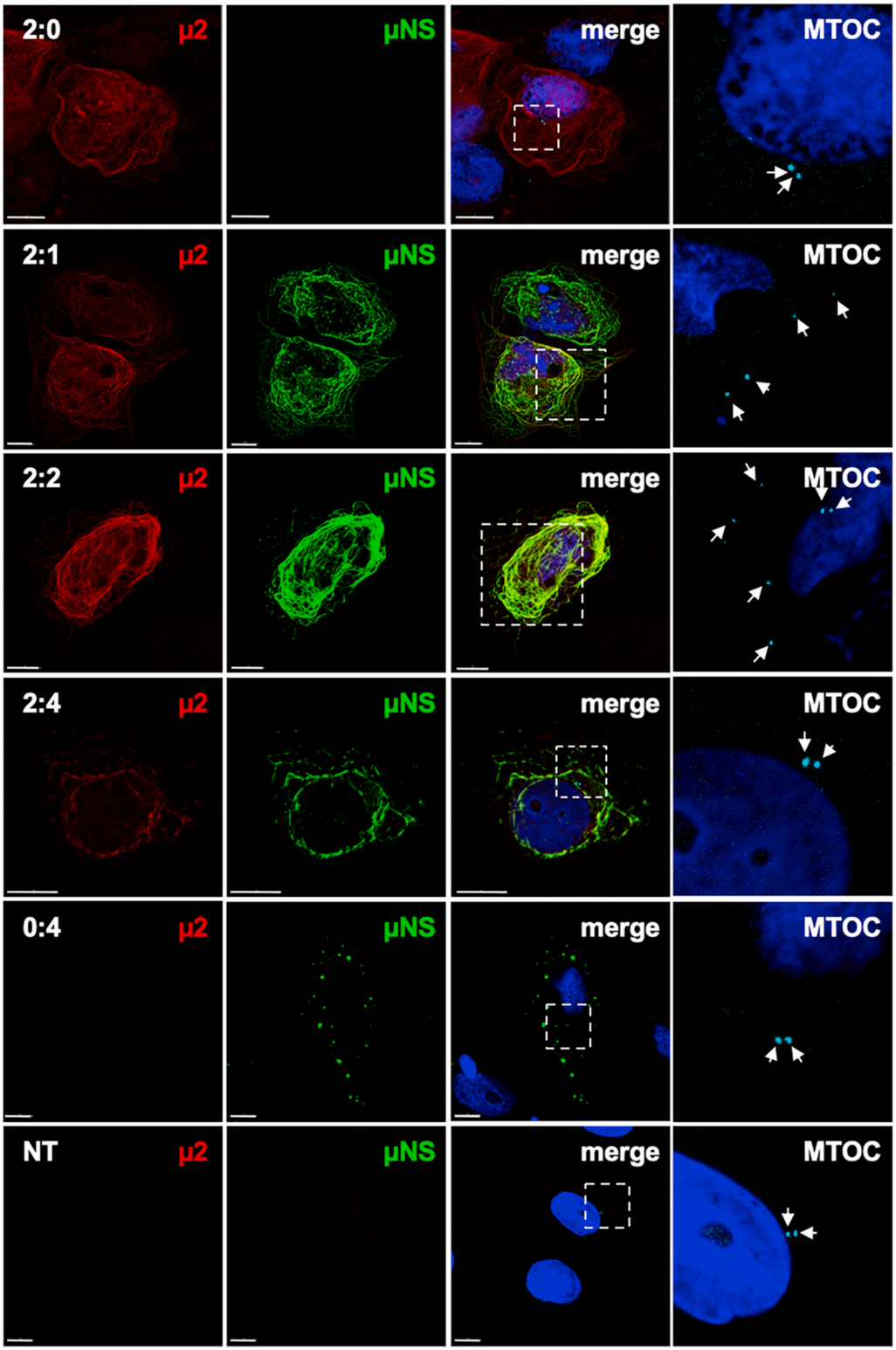

Fig. 6. Centrin redistributes into VFLSs. Confocal maximum intensity projection of VFLSs immunofluorescence. At 24 hpt, CV-1 cells were fixed with methanol and immunostained with specific antibodies for the detection of μ2 (red), μNS (green), and centrin (cyan). Nuclei were stained with DAPI (blue). The third column shows a merged image. The dashed white open boxes correspond to magnified images in the fourth column. White arrowheads point to γ-tubulin localization. NT, non-transfected cells. The μ2/μN transfection ratios are indicated. Scale bar is 10 μm.

obtained by PCR amplification of pBS-TasA-mCherry (Vogt et al., 2016) with specific primers to insert in-frame *Sal*I and STOP codon/*Xma*I, followed by ligation in those sites in pCI-Neo.

All of the oligonucleotides were obtained from Microsynth AG, Switzerland, and the sequences are available upon request.

4.4. Immunofluorescence

CV-1 cells were seeded the day before transfection or infection at a density of 1×10^5 cells per well into 24 multiwell-plates. Cells were transfected with lipofectamine®2000 (Life Technologies) as described

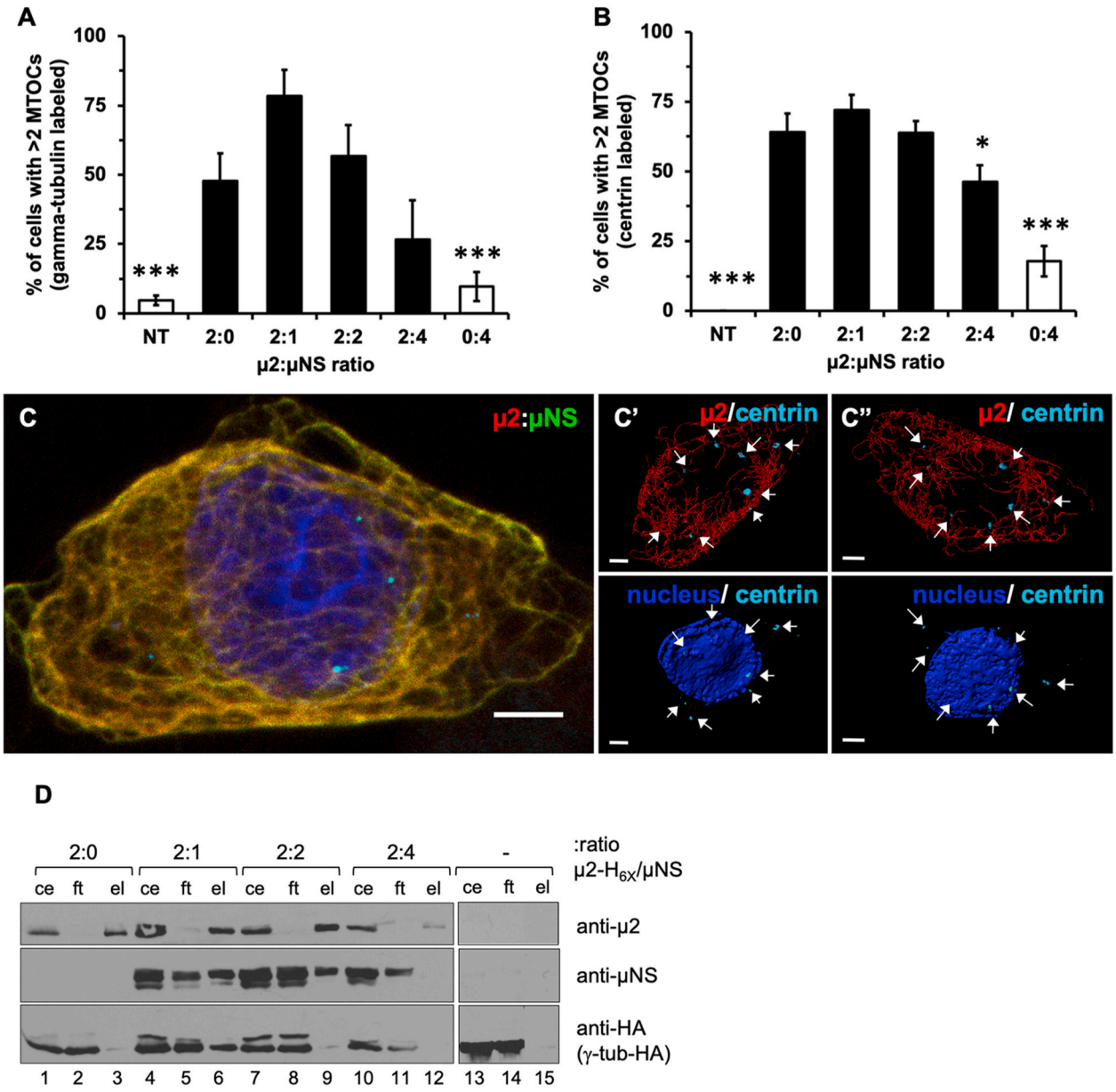

Fig. 7. MTOCs in VFLS increase in number at a specific μ2/μNS ratio. (A and B) The plot of the percentage of cells showing more than two MTOC-like structures (> 2 MTOCs) at each of the indicated ratios of the μ2 and μNS expression plasmids. > 75 cells per sample were analyzed. T-test, (***) $p < 0.001$. Confocal maximum intensity projection (C) and three-dimensional reconstruction (C′, C″) of immunofluorescence staining of VFLS at a μ2/μNS transfection ratio of 2:1. At 24 hpt, CV-1 cells were fixed and immunostained for the detection of μ2 (anti-μ2, red), μNS (anti-μNS, green) and centrin (C, C′ and C″) (anti-centrin, cyan). Three-dimensional reconstruction top (C′) and bottom (C″) show localization of γ-tubulin or centrin with μ2 and nucleus. White arrows point to γ-tubulin and centrin *punctae*. Scale bar is 5 μm. (D) Immunoblot of nickel resin pulled-down extract from cells co-expressing γ-tubulin-HA, μ2-histidine-tagged (H_{6X}-μ2), and μNS (ce, cellular extract input; ft, flow-through; el, column eluate). The ratios of transfected μ2-H_{6X} and μNS expression plasmids are indicated. (−) cell expressing only γ-tubulin-HA. The membranes were incubated with anti-μ2 (upper panel), anti-μNS (middle panel) and anti-HA (lower panel).

previously by (Eichwald et al., 2018). For infection of cell monolayers, an MOI of 10 pfu per cell was used. The virus was adsorbed for 1 h at 4 °C, and then DMEM containing 2% FBS was added. Cells were incubated at 37 °C for the indicated times post-infection. When indicated, cells were fixed in cold methanol for 3 min at − 20 °C. Coverslips were permeabilized for 5 min in PBS [137 mM NaCl, 3 mM KCl, 8 mM Na_2HP0_4, 1 mM KH_2P0_4 pH 7.5] containing 0.1% Triton X-100 and blocked for 30 min in PBS containing 1% bovine serum albumin (BSA) for 20 min. Antibodies were diluted in 1% BSA-PBS and incubated for 45 min at room temperature in a humidified chamber. Nuclei were stained with 70 nM 4,6-diamino-2-phenylindole (DAPI) (Molecular Probes, Invitrogen, USA). Cells were mounted in Prolong Gold (Molecular Probes). Images were acquired using a CSLM (Leica, DM 5500Q) equipped with 63 × 1.3 oil objective or a Nikon Eclipse TE 2000-U fluorescence microscope. The data were analyzed and processed with Leica Application Suite (Mannheim, Germany), the Imaris software package (Bitplane, Switzerland), and ImageJ version 2.0.0-rc69/1.52p.

The intensity profile of a linear region of interest (LROI) was obtained using the ImageJ plot profile tool. The data were plotted using Microsoft Excel for MAC version 16.37. The co-localization value was obtained by calculating the area below the curve of intensity profiles of both μ2 *punctae*-prolongations and other proteins. For this purpose, the Image J magic wand tool was used to provide the grey value intensity for each point, from which a protein signal percentage was obtained on the occupied μ2 *punctae*-prolongation area below the curve. The average value of untreated samples was considered as value of 1 to

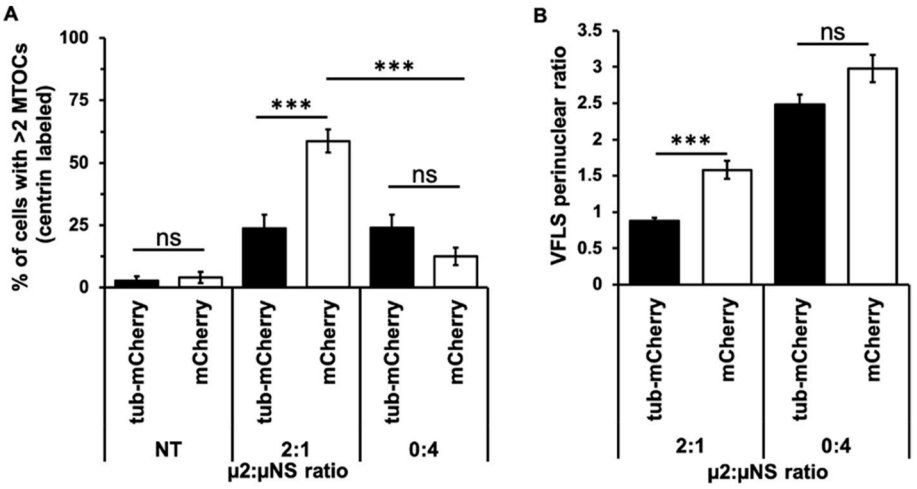

Fig. 8. β-tubulin-mCherry overexpression impairs the re-localization of centrin into VFLS. At 24 hpt, CV-1 cells expressing µ2, µNS, and β-tubulin-mCherry or mCherry were fixed and immunostained for µ2 and µNS, processed for data acquisition hand quantified as described in Materials and Methods. (A) plot of the percentage of µ2/µNS transfected cells with more than two MTOCs per cell when co-expressed with β-tubulin-mCherry (tub-mCherry) (black bars) or mCherry (white bars). (B) Plot for perinuclear condensation of VFLSs at the indicated µ2/µNS ratios when co-expressed with β-tubulin-mCherry (black bars) or mCherry (white bars). All data is presented as mean ± SEM, t-student test, two tail paired, (***) $p < 0.0001$, (ns) $p > 0.05$; number > 70 cells.

determine the relative co-localization to µ2-*punctae*. For confocal data, maximum intensity projections were obtained from Z-stack images acquired by high-resolution CLSM. Subsequently, 3D-reconstructions were performed using surface and filament algorithms from the surpass model of the Imaris 7.0 software (Bitplane, Switzerland). Images were prepared for publication using Microsoft®PowerPoint® 2019 for MAC, version 16.35.

4.5. Determination of perinuclear condensation and quantification of MTOC structures

The condensation of the VFLS to the perinuclear region was expressed as [(F–N)/N] ratio, where F is the area of distribution of the VFs and N is the nuclear area determined using Image J version 2.0.0-rc69/1.52p. For the quantification of MTOCs, confocal maximum intensity projection images were used to sort cells showing VFLS with more than two MTOC like structures. Values, statistical analysis, and two tail-paired Student's tests were performed with Microsoft® Excel 2019 for MAC, version 16.35, as described previously (Eichwald et al., 2012).

4.6. Pull-down assay

1.5×10^6 CV-1 cells were infected with vvT7.3 at an MOI of 10 pfu/cell before transfection with 1 µg pCI-γ-tubulin-HA, 0.5 µg pCI-µ2 (T1L)-H_{6X} and 0.25–1 µg pCI-µNS(T1L) using 18 µl lipofectamine® 2000 (Life Technologies) according to the manufacturer instructions. At 15 hpt, cells were crosslinked with 600 µM dithiol (succinimidyl propionate) in PBS for 20 min on ice. Cells were incubated twice with quenching buffer (50 mM Tris-HCl pH 8.0, 150 mM NaCl) for 3 min on ice. The cell lysates were prepared in 180 µl of TNN buffer (100 mM Tris-HCl pH 8.0, 250 mM NaCl, 0.5% NP-40, 1X HALT phosphatase inhibitor cocktail (Thermo Fischer Scientific) and cOmplete™ protease inhibitor cocktail (Roche)) as described previously (Buttafuoco et al., 2020). The cellular extract was loaded onto 50 µl of PerfectPro Ni-NTA agarose (5 PRIME, Germany) equilibrated in 25 mM imidazole in PBS. Samples were processed and analyzed, as described by (Eichwald et al., 2017).

CRediT authorship contribution statement

Catherine Eichwald: Conceptualization, Data curation, Formal analysis, Investigation, Methodology, Project administration, Resources, Software, Supervision, Writing - original draft, Writing - review & editing. **Mathias Ackermann:** Funding acquisition, Writing - review & editing. **Cornel Fraefel:** Funding acquisition, Writing - review & editing.

Declaration of competing interest

The authors declare that they have no known competing financial interests or personal relationships that could have appeared to influence the work reported in this paper.

Acknowledgments

We thank Urs Greber, Max L. Nibert, and Karl Munger for the reagents described in the text. We thank Max L. Nibert for critical reading and discussion of the manuscript.

This work was supported by a private donation of the late Prof. Dr. Robert Wyler to M.A (F-52601-10-01) and by general funds allocated to C.F. by the University of Zurich.

Appendix A. Supplementary data

Supplementary data to this article can be found online at https://doi.org/10.1016/j.virol.2020.07.008.

References

Akoumianaki, T., Kardassis, D., Polioudaki, H., Georgatos, S.D., Theodoropoulos, P.A., 2009. Nucleocytoplasmic shuttling of soluble tubulin in mammalian cells. J. Cell Sci. 122, 1111–1118.

Aldaz, H., Rice, L.M., Stearns, T., Agard, D.A., 2005. Insights into microtubule nucleation from the crystal structure of human gamma-tubulin. Nature 435, 523–527.

Alushin, G.M., Lander, G.C., Kellogg, E.H., Zhang, R., Baker, D., Nogales, E., 2014. High-resolution microtubule structures reveal the structural transitions in αβ-tubulin upon GTP hydrolysis. Cell 157, 1117–1129.

Angelini, M.M., Akhlaghpour, M., Neuman, B.W., Buchmeier, M.J., 2013. Severe acute respiratory syndrome coronavirus nonstructural proteins 3, 4, and 6 induce double-membrane vesicles. mBio 4, e00524.

Arnold, M.M., Murray, K.E., Nibert, M.L., 2008. Formation of the factory matrix is an important, though not a sufficient function of nonstructural protein mu NS during reovirus infection. Virology 375, 412–423.

Baas, P.W., Ahmad, F.J., 1992. The plus ends of stable microtubules are the exclusive nucleating structures for microtubules in the axon. J. Cell Biol. 116, 1231–1241.

Becker, M.M., Goral, M.I., Hazelton, P.R., Baer, G.S., Rodgers, S.E., Brown, E.G., Coombs, K.M., Dermody, T.S., 2001. Reovirus sigmaNS protein is required for nucleation of viral assembly complexes and formation of viral inclusions. J. Virol. 75, 1459–1475.

Broering, T.J., Kim, J., Miller, C.L., Piggott, C.D., Dinoso, J.B., Nibert, M.L., Parker, J.S., 2004. Reovirus nonstructural protein mu NS recruits viral core surface proteins and entering core particles to factory-like inclusions. J. Virol. 78, 1882–1892.

Broering, T.J., Parker, J.S., Joyce, P.L., Kim, J., Nibert, M.L., 2002. Mammalian reovirus nonstructural protein microNS forms large inclusions and co-localizes with reovirus microtubule-associated protein micro2 in transfected cells. J. Virol. 76, 8285–8297.

Buttafuoco, A., Michaelsen, K., Tobler, K., Ackermann, M., Fraefel, C., Eichwald, C., 2020. Conserved rotavirus NSP5 and VP2 domains interact and affect viroplasm. J. Virol. 94.

Chandran, K., Nibert, M.L., 1998. Protease cleavage of reovirus capsid protein mu1/mu1C is blocked by alkyl sulfate detergents, yielding a new type of infectious subvirion particle. J. Virol. 72, 467–475.

Coombs, K.M., 1996. Identification and characterization of a double-stranded RNA-

reovirus temperature-sensitive mutant defective in minor core protein mu2. J. Virol. 70, 4237–4245.
Eichwald, C., Ackermann, M., Nibert, M.L., 2018. The dynamics of both filamentous and globular mammalian reovirus viral factories rely on the microtubule network. Virology 518, 77–86.
Eichwald, C., Arnoldi, F., Laimbacher, A.S., Schraner, E.M., Fraefel, C., Wild, P., Burrone, O.R., Ackermann, M., 2012. Rotavirus viroplasm fusion and perinuclear localization are dynamic processes requiring stabilized microtubules. PloS One 7, e47947.
Eichwald, C., Kim, J., Nibert, M.L., 2017. Dissection of mammalian orthoreovirus μ2 reveals a self-associative domain required for binding to microtubules but not to factory matrix protein μNS. PloS One 12, e0184356.
Fuerst, T.R., Niles, E.G., Studier, F.W., Moss, B., 1986. Eukaryotic transient-expression system based on recombinant vaccinia virus that synthesizes bacteriophage T7 RNA polymerase. Proc. Natl. Acad. Sci. U. S. A. 83, 8122–8126.
Goodson, H.V., Jonasson, E.M., 2018. Microtubules and microtubule-associated proteins. Cold Spring Harb Perspect Biol 10, a022608.
Hossain, D., Ferreira Barbosa, J.A., Cohen, É., Tsang, W.Y., 2018. HIV-1 Vpr hijacks EDD-DYRK2-DDB1. J. Biol. Chem. 293, 9448–9460.
Irvin, S.C., Zurney, J., Ooms, L.S., Chappell, J.D., Dermody, T.S., Sherry, B., 2012. A single-amino-acid polymorphism in reovirus protein μ2 determines repression of interferon signaling and modulates myocarditis. J. Virol. 86, 2302–2311.
Ivanovic, T., Boulant, S., Ehrlich, M., Demidenko, A.A., Arnold, M.M., Kirchhausen, T., Nibert, M.L., 2011. Recruitment of cellular clathrin to viral factories and disruption of clathrin-dependent trafficking. Traffic 12, 1179–1195.
Janke, C., Bulinski, J.C., 2011. Post-translational regulation of the microtubule cytoskeleton: mechanisms and functions. Nat. Rev. Mol. Cell Biol. 12, 773–786.
Kaufer, S., Coffey, C.M., Parker, J.S., 2012. The cellular chaperone hsc70 is specifically recruited to reovirus viral factories independently of its chaperone function. J. Virol. 86, 1079–1089.
Kim, J., Parker, J.S., Murray, K.E., Nibert, M.L., 2004. Nucleoside and RNA triphosphatase activities of orthoreovirus transcriptase cofactor mu2. J. Biol. Chem. 279, 4394–4403.
Knowlton, J.J., Fernández de Castro, I., Ashbrook, A.W., Gestaut, D.R., Zamora, P.F., Bauer, J.A., Forrest, J.C., Frydman, J., Risco, C., Dermody, T.S., 2018. The TRiC chaperonin controls reovirus replication through outer-capsid folding. Nat Microbiol 3, 481–493.
Kollman, J.M., Polka, J.K., Zelter, A., Davis, T.N., Agard, D.A., 2010. Microtubule nucleating gamma-TuSC assembles structures with 13-fold microtubule-like symmetry. Nature 466, 879–882.
L'Hernault, S.W., Rosenbaum, J.L., 1985. Chlamydomonas alpha-tubulin is post-translationally modified by acetylation on the epsilon-amino group of a lysine. Biochemistry 24, 473–478.
LeDizet, M., Piperno, G., 1987. Identification of an acetylation site of Chlamydomonas alpha-tubulin. Proc. Natl. Acad. Sci. U. S. A. 84, 5720–5724.
Lindeboom, J.J., Nakamura, M., Hibbel, A., Shundyak, K., Gutierrez, R., Ketelaar, T., Emons, A.M., Mulder, B.M., Kirik, V., Ehrhardt, D.W., 2013. A mechanism for reorientation of cortical microtubule arrays driven by microtubule severing. Science 342, 1245533.
Lüders, J., Stearns, T., 2007. Microtubule-organizing centres: a re-evaluation. Nat. Rev. Mol. Cell Biol. 8, 161–167.
Mainou, B.A., Dermody, T.S., 2011. Src kinase mediates productive endocytic sorting of reovirus during cell entry. J. Virol. 85, 3203–3213.
Mainou, B.A., Zamora, P.F., Ashbrook, A.W., Dorset, D.C., Kim, K.S., Dermody, T.S., 2013. Reovirus cell entry requires functional microtubules. mBio 4, e00405.
Matov, A., Applegate, K., Kumar, P., Thoma, C., Krek, W., Danuser, G., Wittmann, T., 2010. Analysis of microtubule dynamic instability using a plus-end growth marker. Nat. Methods 7, 761–768.
Miller, C.L., Arnold, M.M., Broering, T.J., Hastings, C.E., Nibert, M.L., 2010. Localization of mammalian orthoreovirus proteins to cytoplasmic factory-like structures via nonoverlapping regions of microNS. J. Virol. 84, 867–882.
Miller, C.L., Broering, T.J., Parker, J.S., Arnold, M.M., Nibert, M.L., 2003. Reovirus sigma NS protein localizes to inclusions through an association requiring the mu NS amino terminus. J. Virol. 77, 4566–4576.
Miller, Cathy L., Parker, John S.L., Dinoso, Jason B., Piggot, Caroline D.S., Perron, Michel J., Nibert, Max L., 2004. Increased ubiquitination and other covariant phenotypes attributed to a strain- and temperature-dependent defect of reovirus core protein mu2. Journal of Virology 78 (19), 10291–10302. https://doi.org/10.1128/JVI.78.19.10291-10302.2004.
Nguyen, C.L., Eichwald, C., Nibert, M.L., Münger, K., 2007. Human papillomavirus type 16 E7 oncoprotein associates with the centrosomal component gamma-tubulin. J. Virol. 81, 13533–13543.
Noble, S., Nibert, M.L., 1997. Core protein mu2 is a second determinant of nucleoside triphosphatase activities by reovirus cores. J. Virol. 71, 7728–7735.
Parker, J.S., Broering, T.J., Kim, J., Higgins, D.E., Nibert, M.L., 2002. Reovirus core protein mu2 determines the filamentous morphology of viral inclusion bodies by interacting with and stabilizing microtubules. J. Virol. 76, 4483–4496.
Pasdeloup, D., Labetoulle, M., Rixon, F.J., 2013. Differing effects of herpes simplex virus 1 and pseudorabies virus infections on centrosomal function. J. Virol. 87, 7102–7112.
Piperno, G., LeDizet, M., Chang, X.J., 1987. Microtubules containing acetylated alpha-tubulin in mammalian cells in culture. J. Cell Biol. 104, 289–302.
Procter, D.J., Banerjee, A., Nukui, M., Kruse, K., Gaponenko, V., Murphy, E.A., Komarova, Y., Walsh, D., 2018. The HCMV assembly compartment is a dynamic Golgi-derived MTOC that controls nuclear rotation and virus spread. Dev. Cell 45, 83–100 e107.
Rhim, J.S., Jordan, L.E., Mayor, H.D., 1962. Cytochemical, fluorescent-antibody and electron microscopic studies on the growth of reovirus (ECHO 10) in tissue culture. Virology 17, 342–355.
Rogalski, A.A., Singer, S.J., 1984. Associations of elements of the Golgi apparatus with microtubules. J. Cell Biol. 99, 1092–1100.
Roostalu, J., Surrey, T., 2017. Microtubule nucleation: beyond the template. Nat. Rev. Mol. Cell Biol. 18, 702–710.
Salisbury, J.L., 2007. A mechanistic view on the evolutionary origin for centrin-based control of centriole duplication. J. Cell. Physiol. 213, 420–428.
Sanchez, A.D., Feldman, J.L., 2017. Microtubule-organizing centers: from the centrosome to non-centrosomal sites. Curr. Opin. Cell Biol. 44, 93–101.
Shah, P.N.M., Stanifer, M.L., Höhn, K., Engel, U., Haselmann, U., Bartenschlager, R., Kräusslich, H.G., Krijnse-Locker, J., Boulant, S., 2017. Genome packaging of reovirus is mediated by the scaffolding property of the microtubule network. Cell Microbiol. 19, e12765.
Soppina, V., Herbstman, J.F., Skiniotis, G., Verhey, K.J., 2012. Luminal localization of α-tubulin K40 acetylation by cryo-EM analysis of fab-labeled microtubules. PloS One 7, e48204.
Srayko, M., O'toole, E.T., Hyman, A.A., Müller-Reichert, T., 2006. Katanin disrupts the microtubule lattice and increases polymer number in C. elegans meiosis. Curr. Biol. 16, 1944–1949.
Stebbing, R.E., Irvin, S.C., Rivera-Serrano, E.E., Boehme, K.W., Ikizler, M., Yoder, J.A., Dermody, T.S., Sherry, B., 2014. An ITAM in a nonenveloped virus regulates activation of NF-κB, induction of beta interferon, and viral spread. J. Virol. 88, 2572–2583.
Tyler, K.L., Bronson, R.T., Byers, K.B., Fields, B., 1985. Molecular basis of viral neurotropism: experimental reovirus infection. Neurology 35, 88–92.
Vertii, A., Hehnly, H., Doxsey, S., 2016. The Centrosome, a multitalented renaissance organelle. Cold Spring Harb Perspect Biol 8, a025049.
Virgin, H.W., Mann, M.A., Fields, B.N., Tyler, K.L., 1991. Monoclonal antibodies to reovirus reveal structure/function relationships between capsid proteins and genetics of susceptibility to antibody action. J. Virol. 65, 6772–6781.
Vogt, C.M., Schraner, E.M., Aguilar, C., Eichwald, C., 2016. Heterologous expression of antigenic peptides in *Bacillus subtilis* biofilms. Microb. Cell Factories 15, 137.
Wiener, J.R., Bartlett, J.A., Joklik, W.K., 1989. The sequences of reovirus serotype 3 genome segments M1 and M3 encoding the minor protein mu 2 and the major nonstructural protein mu NS, respectively. Virology 169, 293–304.
Wileman, T., Netherton, C.L., Powell, P.P., 2016. Virus factories and mini-organelles generated for virus replication. Encyclopedia of Cell Biology 2, 819–827.
Zheng, Y., Wong, M.L., Alberts, B., Mitchison, T., 1995. Nucleation of microtubule assembly by a gamma-tubulin-containing ring complex. Nature 378, 578–583.
Zurney, J., Kobayashi, T., Holm, G.H., Dermody, T.S., Sherry, B., 2009. Reovirus mu2 protein inhibits interferon signaling through a novel mechanism involving nuclear accumulation of interferon regulatory factor 9. J. Virol. 83, 2178–2187.